

Iterative RF pulse design for multi-dimensional, small-tip-angle selective excitation

Chun-yu Yip¹, Jeffrey A. Fessler^{1,2}, Douglas C. Noll²

¹Department of Electrical Engineering and Computer Science, University of Michigan, Ann Arbor, MI

²Department of Biomedical Engineering, University of Michigan, Ann Arbor, MI

Revised draft submitted to Magnetic Resonance in Medicine

April 2005

Running head: Iterative RF pulse design

Manuscript word count: 5000 words (approximate)

Correspondence to: Chun-yu Yip

Address: Functional MRI Laboratory, University of Michigan, 2360 Bonisteel Ave, Ann Arbor, MI 48109-2108, USA.

Telephone number: 734-647-1996

Fax number: 734-938-4218

Email address: chunyuy@umich.edu

Grant sponsor: NIH DA15410

ABSTRACT

The excitation k-space perspective on small-tip-angle selective excitation has facilitated RF pulse designs in a range of MR applications. In this paper, k-space based design of multi-dimensional RF pulses is formulated as a quadratic optimization problem, and solved efficiently by the iterative conjugate gradient algorithm. Compared to conventional design approaches such as the conjugate-phase method, the new design approach is beneficial in several regards. It generally produces more accurate excitation patterns. The improvement is particularly significant when k-space is undersampled, and it can potentially shorten pulse lengths. Prominent accuracy improvement is also observed where large off resonance gradients are present. Further boost in excitation accuracy can be accomplished in regions of interest, if specified together with “don’t-care” regions. Density compensation function is no longer required. In addition, regularization techniques allow control over integrated and peak pulse power.

Key words: iterative pulse design, small tip angle, selective excitation, excitation k-space

INTRODUCTION

The design of RF pulses for multi-dimensional, small-tip-angle selective excitation is facilitated by the *excitation k-space* perspective, developed by Pauly *et al.* [1] under the small-tip-angle approximation to the Bloch equation. K-space based selective excitation has been used in a range of MR applications, such as functional MRI artifact correction [2], brain imaging with reduced field of view (FOV) [3], blood velocity measurement [4], parallel excitation using multiple transmit coils [5, 6], and excitation inhomogeneity correction [7]. The k-space perspective has been popular because it provides a fairly accurate linear Fourier relationship between the time-varying gradient, RF waveforms and the resulting transverse excitation pattern. The Fourier relationship can also be established for rotation angles, possibly large, provided that certain symmetry conditions are satisfied [8].

A common approach to small-tip-angle RF pulse design is to predetermine the gradient waveforms and thus the k-space trajectory, and then obtain the complex-valued RF waveform by sampling the Fourier transform of the desired excitation pattern along the trajectory. Afterwards, the sample values are compensated for density variation in the trajectory. Some researchers have designed pulses by adopting the conjugate-phase (CP) approach from image reconstruction [9, 10], which accounts for off resonance and thus can correct for it to some extent [11, 12].

These conventional approaches are non-ideal in several regards. First, in terms of minimizing excitation error, they generally produce pulses that are suboptimal even with respect to just the linear design model. This design suboptimality is an eradicable source of excitation error, on top of the intractable amount due to the small-tip-angle approximation underlying excitation k-space. The excitation error due to design suboptimality is particularly large when the trajectory undersamples k-space, or when large spatial variations of off resonance are present [11]. To compensate for the effects of off resonance gradients to some extent, Noll *et al.* [13] suggested a sophisticated density compensation function (DCF) in the CP method, but it is spatially variant and may not be readily extended to the excitation case. In fact, accurate DCF evaluation can generally be difficult and time consuming (see, for example, [14]). Erroneous DCF evaluation contributes significantly to excitation error.

Besides suboptimality, the current design approaches can handle neither the secondary objective of minimizing integrated RF power due to Specific Absorption Rate (SAR) considerations [15, 16], nor the hard constraint of peak RF power due to amplifier limitation [17]. Also, they are unable to exploit the possibility of assigning spatial weighting to excitation error. These issues suggest that there is room for improvement in small-tip-angle RF pulse design methodology, which would benefit current applications and possibly foster future ones.

The inverse-problem nature of small-tip-angle RF pulse design suggests that an optimization approach can be beneficial. In fact, a range of optimization schemes have been used by researchers to design slice-selective 90-degree, inversion, and spin-echo pulses (for example, [15–20]). Those optimal pulses, designed with respect to the exact Bloch-equation system, achieved very accurate slice profiles. It is a natural extension to apply some of those schemes to the small-tip-angle design problem. Another inspiration for a better design method is the recent

iterative image reconstruction algorithms [21, 22], which are also optimization schemes. Iterative reconstruction methods produce improved image quality relative to the CP and gridding methods [21–23]. The analogy between image reconstruction and small-tip-angle RF pulse design [11] suggests that similar iterative optimization schemes can be applied to the latter.

In this context, we propose that small-tip-angle RF pulses can be designed via minimization of a quadratic cost function that consists of an excitation error term and regularization terms that control the integrated and peak RF power. The minimization problem can be solved iteratively via the conjugate gradient (CG) method [22]. Off resonance during excitation, particularly in the case of long pulses, has significant impact on the excitation accuracy [11, 12]. Thus, its effects are included in our design model.

In the following section we formulate small-tip-angle RF pulse design as an optimization problem, followed by a discussion of its numerical solution. We then present Bloch equation simulation results, showing quantitatively the benefits of the iterative design method, in terms of excitation accuracy when excitation k-space is undersampled or off resonance is present. We also investigated the tradeoff between excitation accuracy and RF power. Finally, we present results from scanner experiments.

THEORY

Let us define complex function $M(\mathbf{x}, b)$ as the transverse magnetization pattern resulting from the Bloch equation, with input complex RF pulse envelope $b(t)$ and predetermined real gradient waveforms $\mathbf{g}(t) = [g_x(t)g_y(t)g_z(t)]^T$, $t \in [0, T]$. We assume that all magnetization is initially fully relaxed and aligned with $+z$ axis, and has equilibrium magnitude M_o . For tip angles between 0 and 90 degrees, the complex representation can unambiguously specify magnetization. In the small-tip-angle regime, an optimal RF pulse can be designed via minimizing a cost function that includes an excitation error measure, and a pulse energy term, which allows for a soft constraint on the integrated RF pulse power:

$$b_{opt} = \arg \min_b \left\{ \int_{-\infty}^{\infty} |M(\mathbf{x}; b) - D(\mathbf{x})|^2 W(\mathbf{x}) d\mathbf{x} + \beta \int_0^T |b(t)|^2 dt \right\}, \quad (1)$$

subject to the peak RF power hard constraint

$$|b(t)|^2 \leq C \quad , \quad t \in [0, T]. \quad (2)$$

In Eq. (1), complex function $D(\mathbf{x})$ is the desired magnetization pattern, real function $W(\mathbf{x})$ is a user-defined error weighting pattern that can cover the FOV or any arbitrary ROIs, and β is a regularization parameter that should be tuned based on SAR considerations. C is a certain constant dependent on the RF amplifier peak power limitation. A similar version of this problem for large-tip excitation was solved in [15–17] for the one-dimensional and constant-gradient case, but it was a difficult and time-consuming optimization problem due to the Bloch equation

nonlinearity. In the small-tip-angle regime, linearization of the Bloch equation can reduce Eq. (1) to a more easily solvable form.

Using the small-tip-angle approximation, Pauly *et al.* [1] derived that $M(\mathbf{x}; b)$ can be approximated by a Fourier integral, and off resonance during excitation can be easily incorporated by an extra exponential factor [11, 12]:

$$M(\mathbf{x}; b) \approx i\gamma M_o \int_0^T b(t) e^{i\mathbf{k}(t) \cdot \mathbf{x} + i\Delta\omega(\mathbf{x})[t-T]} dt, \quad (3)$$

where γ denotes the gyromagnetic ratio, $\Delta\omega(\mathbf{x})$ represents resonance frequency offsets, and $\mathbf{k}(t)$ is any realizable excitation k-space trajectory given by the integral of the remaining gradient area:

$$\mathbf{k}(t) = -\gamma \int_t^T \mathbf{g}(\tau) d\tau. \quad (4)$$

An RF pulse is generally defined discretely in a pulse sequence, processed by a Digital-to-Analog (D/A) converter, and then played out in the coil via RF circuitry. Let $b_j, j = 0, \dots, N_t - 1$ be the pulse samples in the pulse sequence, and Δt be the sampling period. If the temporal point spread function¹ in the pulse physically played out is narrow, then we can approximate Eq. (3) as

$$M(\mathbf{x}; b) \approx i\gamma M_o \sum_{j=0}^{N_t-1} b_j e^{i\mathbf{k}(t_j) \cdot \mathbf{x} + i\Delta\omega(\mathbf{x})[t_j-T]} \Delta t. \quad (5)$$

We sample M at user-selected spatial locations $\{\mathbf{x}_i\}_{i=0}^{N_s-1}$, and express Eq. (5) in matrix-vector multiplication form:

$$\mathbf{m} \approx \mathbf{A} \mathbf{b} \quad (6)$$

where $\mathbf{m} = [M(\mathbf{x}_0; b) \dots M(\mathbf{x}_{N_s-1}; b)]^T$, $\mathbf{b} = [b_0 \dots b_{N_t-1}]^T$, and the elements of the $N_s \times N_t$ system matrix \mathbf{A} are

$$a_{i,j} = i\gamma M_o e^{i\mathbf{k}(t_j) \cdot \mathbf{x}_i + i\Delta\omega(\mathbf{x}_i)[t_j-T]} \Delta t. \quad (7)$$

Now, we can obtain the RF pulse samples by solving

$$\hat{\mathbf{b}} = \arg \min_{\mathbf{b}} \{ \|\mathbf{A}\mathbf{b} - \mathbf{d}\|_{\mathbf{W}}^2 + \beta \mathbf{b}' \mathbf{b} \}, \quad (8)$$

subject to

$$|b_j|^2 \leq C, \quad j = 0, \dots, N_t - 1, \quad (9)$$

in which \mathbf{d} is a vector that contains samples of the desired pattern at the corresponding spatial locations, $'$ denotes complex conjugate transpose, and \mathbf{W} is an $N_s \times N_s$ diagonal matrix containing the user-selected error weighting

$\{W(\mathbf{x}_i)\}_{i=0}^{N_s-1}$. The \mathbf{W} -weighted 2-norm denotes $(\mathbf{A}\mathbf{b} - \mathbf{d})'\mathbf{W}(\mathbf{A}\mathbf{b} - \mathbf{d})$. \mathbf{W} can be used to specify spin-free regions as “don’t care” regions.

The dimensions of matrix \mathbf{A} depend on the sample spacing in \mathbf{m} and \mathbf{d} , and the length of the RF pulse being designed. Indeed, sample spacing in \mathbf{m} and \mathbf{d} dictates whether the system of equations $\mathbf{A}\mathbf{b} = \mathbf{d}$ would be overdetermined or underdetermined, when no regularization is applied. We found that it is generally beneficial, in terms of excitation error evaluated over the continuous spatial domain, to sample $D(\mathbf{x})$ finely (with higher resolution than that supported by the trajectory) so that the unregularized design problem $\mathbf{A}\mathbf{b} = \mathbf{d}$ is overdetermined.

We can invoke the Karush-Kuhn-Tucker (KKT) Theorem in non-linear optimization theory [24] to solve Eqs. (8) and (9), as detailed in the appendix. The optimal solution suggests that a magnitude-constrained RF pulse can be designed via

$$\hat{\mathbf{b}} = \arg \min_{\mathbf{b}} \{ \|\mathbf{A}\mathbf{b} - \mathbf{d}\|_{\mathbf{W}}^2 + \beta \mathbf{b}'\mathbf{b} + \mathbf{b}'\mathbf{\Lambda}\mathbf{b} \}, \quad (10)$$

where $\mathbf{\Lambda} = \text{diag}(\lambda_j)$, with $\lambda_j, j = 0, \dots, N_t - 1$ denoting regularization parameters controlling the magnitude of individual RF pulse samples. One can describe $\mathbf{b}'\mathbf{\Lambda}\mathbf{b}$ as a *local regularization* term for controlling peak RF power, whereas $\beta \mathbf{b}'\mathbf{b}$ is the global *Tikhonov regularization* term, often used in other imaging applications, to control integrated RF power. Regularization may degrade the fit between the resulting and desired pattern in exchange for reducing integrated and peak pulse power. The tradeoff can be tuned by the regularization parameters. Slight Tikhonov regularization is generally needed to ensure that pulses are physically realizable.

For a certain set of regularization parameters, the designed pulse can be constraint-violating and thus the parameters have to be incremented. One heuristic approach to search for a good set of parameter values is to iteratively check integrated and peak RF power, increment β in case of integrated power violation and λ_j in case of peak power violation at pulse sample b_j , and then redesign with the new parameter values, until the integrated power is acceptable and the peak power is within amplifier limitation. This “check-and-redesign” process is sensible, because for practical pulse design problems, the RF power constraints are often not violated. The peak power constraint violation may occur at very few time points, if at all. Thus all or most of the regularization parameters can be zero. In such cases, the heuristic approach is computationally economical because it avoids simultaneously solving for the optimizing pulse and KKT multipliers (see Appendix).

For Eq. (10), if the regularization parameter values are fixed, then $\hat{\mathbf{b}} = (\mathbf{A}'\mathbf{W}\mathbf{A} + \mathbf{R})^{-1}\mathbf{A}'\mathbf{W}\mathbf{d}$, where $\mathbf{R} = \mathbf{I}\beta + \mathbf{\Lambda}$. This analytical solution involves a matrix inversion, which is a computationally intensive $O(N_t^3)$ operation. To reduce the complexity, we instead apply the $O(N_t^2)$ iterative conjugate gradient (CG) algorithm [22], which converges to the optimizing pulse over iterations. The complexity reduction can be highly significant for design of long pulses. One can initialize CG with a CP design for a good initial guess. Alternatively, one can initialize with a zero pulse without loss of excitation accuracy, provided that enough iterations are used.

MATERIALS AND METHODS

Pulse computations

RF pulses were computed offline with Matlab 6.5 (MathWorks Inc., Natick, MA). They were spatially selective in the two transverse dimensions. We used, in all cases, single-shot spiral-out excitation k-space trajectories [25], with the following gradient parameters: maximum magnitude = 4 G/cm, maximum slew rate = 18000 G/cm/s, and sampling period = 4 μ s. Unless otherwise stated in specific experiments, we used a trajectory which supported 0.5 cm \times 0.5 cm resolution, and an excitation field of view (XFOV) of 18 cm diameter, resulting in pulse duration of 9.01 ms.

The desired patterns had common resolution of 0.25 cm \times 0.25 cm. In the simulations, the desired pattern was a 15 cm \times 5 cm block, with magnitude 0.5 (unit magnitude corresponded to 90 degree tip angle), perfectly sharp edges, and 0 phase everywhere. Excitation error was equally weighted, either within a circular ROI with 20 cm diameter, or an elliptic reduced ROI, with length of major and minor axes being 18 cm and 12 cm, respectively. Outside the ROIs were “don’t care” regions assigned with 0 error weighting. This setup simulated inner volume excitation of a block inside a human skull for spectroscopic imaging [26], for which the elliptic ROI covered the head within the FOV. Desired patterns and ROIs in the scanner experiments will be detailed in the Scanner Experiments Section.

The CG algorithm in the iterative method was initialized with a zero pulse, and run for 15 iterations for sufficient convergence. Except in Simulation III, we used Tikhonov regularization with $\beta = 2.25$ to avoid physically unrealizable pulse designs. Off resonance was considered in Simulation II and Scanner Experiment II.

For comparison with the iterative method, we used the CP algorithm as the standard. DCFs were calculated based on the Jacobian formula [27]. When resonance frequency offsets are not incorporated, CP is equivalent to the method of sampling the Fourier transform of the desired pattern along the trajectory, provided that there is no interpolation error introduced in the sampling step. Such interpolation error can be made arbitrarily small by zero-padding the target pattern before transformation.

Numerical simulations

To evaluate RF pulses, we performed numerical simulations of the Bloch equation with Matlab. The Bloch simulation was over a two-dimensional grid covering a 20 cm \times 20 cm region, with 0.25 cm \times 0.25 cm resolution. Relaxation effects were ignored. In Simulation II, a field map was incorporated in the Bloch simulator. For each excitation result from the Bloch simulator (\mathbf{m}_{bl}), we calculated the normalized root-mean-square excitation error (NRMSE) with respect to the desired pattern. NRMSE was defined as $\|\mathbf{m}_{bl} - \mathbf{d}\|_{\mathbf{W}} / \|\mathbf{d}\|_{\mathbf{W}}$. Note that in each simulation study, the same \mathbf{W} was used for both the CP and iterative methods, and it covered the same ROI

incorporated in the iterative scheme.

Simulation I: k-space undersampling

The goal of Simulation I was to compare the CP and iterative methods used in conjunction with trajectories that undersample excitation k-space. Spiral-out trajectories being tested covered a fixed range in k-space, while the sampling interval was varied, leading to XFOV diameters ranging from 10 cm to 22 cm. For each XFOV diameter value, we computed the corresponding RF pulse designed via CP, and iterative method with either the circular or elliptic ROI. Gradient and RF pulse waveforms were then fed into the Bloch simulator, and within-ROI NRMSE was computed.

Simulation II: off resonance correction

In Simulation II we compared the design methods' capability of correcting for off resonance during excitation. In the Bloch simulator, we incorporated a field map with flat regions in the center (+60 Hz) and background (-60 Hz), bridged by a linear transition region (Fig. 1). The width of the linear transition region was varied to represent different roughness of the field map, with the central +60 Hz region fixed. For each transition steepness value, we simulated pulses designed with field-map-incorporated CP and iterative method, using either the circular or elliptic ROI. In all cases, NRMSE was evaluated *only* within the transition region inside the ROIs.

Simulation III: RF pulse power management

Simulation III demonstrated the use of regularization for controlling integrated and peak RF power. The iteratively-designed pulse in Simulation I, with circular ROI, XFOV = 13 cm and $\beta = 2.25$, was treated as the original pulse. In two separate studies, we investigated reducing its integrated power by 50% and the peak power by 75%.

For integrated power reduction, the original pulse was redesigned via iteratively incrementing β by 1.0 and rerunning the iterative scheme, until the integrated power was below 50% of the original. For peak power reduction, the original pulse was redesigned via iteratively locating pulse samples which violated the peak magnitude constraint (50% of the original peak), incrementing the local regularization parameters $\{\lambda_j\}$ at those violation points by 1.0, and rerunning the iterative scheme using the updated parameter values, until the peak RF power was below 50% of the original. As the local regularization parameters were varied, we kept the original Tikhonov regularization ($\beta = 2.25$).

We compared the NRMSE penalty induced by regularization, to that by simply scaling the original pulse by $1/\sqrt{2}$ or clipping at half of its maximum magnitude.

Scanner experiments

Scanner experiments were performed on a GE 3 T Signa Scanner (GE Healthcare, Milwaukee, WI), using a spherical homogeneous water phantom (GE Healthcare). Two-dimensional excitation patterns were imaged by a spin-echo (SE) spiral-out pulse sequence, in which the slice-selective sinc pulse was replaced by the two-dimensional pulse designs. The 180-degree pulse was slice-selective for refocusing the slice being imaged. Prescans for ROI and field map (Experiment II) were acquired by a gradient-echo (GRE) spiral-out sequence. Eight acquisition interleaves were used in all sequences to minimize the off resonance effect during acquisition. Common imaging parameters were as follows: slice thickness = 3.0 mm, FOV = 20 cm; matrix size = 64×64 ; Repetition Time (TR) = 1 s; Echo Time (TE) = 40 ms (SE), 7.6 ms (GRE). In each of the two experiments, flip angles of patterns being compared were matched via proper scaling of the pulses. For the two-dimensional pulses, gradient waveforms for excitation were shifted forward by $145 \mu\text{s}$ to compensate for the delay between RF and gradient channels. Images were reconstructed from the scanner data using a fast implementation of the off-resonance compensated CP method [9]. It used field maps estimated from two images acquired with a TE difference of 2 ms [28]. By using a SE sequence with multiple interleaves and an off resonance compensated reconstruction scheme, image artifacts due to off resonance during acquisition were insignificant.

Experiment I: variable-density trajectory

Variable-density spiral trajectories [29, 30], which undersample k-space regionally, can be useful for pulse length reduction. We investigated whether aliasing could be alleviated when those trajectories were used in conjunction with the iterative design method. Excitation patterns, produced by an identical variable-density trajectory but different RF pulse designs, were imaged and compared.

The variable-density spiral-out trajectory we deployed adequately sampled excitation k-space near the origin (XFOV = 18 cm), and undersampled by a factor of 2.5 in the high-frequency region (Fig. 2). Pulse length was 4.65 ms, and durations of the adequate-sampling and transition (from adequate-sampling to under-sampling) segments were 1.0 ms and 0.8 ms, respectively. To simulate ROI determination in human scanning, we prescanned the phantom with a GRE spiral sequence with a slice-selective sinc pulse, and thresholded the resulting image at 0.3 of its maximum magnitude. CP and (ROI-incorporated) iterative methods were then applied to compute two RF pulses for the desired pattern, which was a uniform disc with 6 cm diameter and sharp edges. Selective excitation of discs is useful in applications such as inner volume excitation [26] and two-dimensional navigator pulses [31].

Experiment II: off resonance correction

This experiment compared the design methods' capability of correcting for excitation distortion due to off resonance during pulse application. Three ferromagnetic metal pieces were attached to the phantom surface to create main field inhomogeneity. With the same 9.01 ms trajectory as in the simulations, one pulse was designed using the iterative method *without* field map incorporation, whereas two other pulses were designed using CP and iterative methods, both *with* field map incorporation. As in the previous experiment, we prescanned the phantom and performed image thresholding to determine the ROI. The resulting excitation patterns were then imaged and compared.

The field map was estimated from two GRE images [28], with TE values of 7.60 ms and 8.60 ms. We masked it with the ROI, and then smoothed it using a regularized weighted least-squares method [32] before incorporation. The desired pattern was an arbitrary "stripes" pattern, which covered the entire phantom and demonstrated off resonance correction well.

RESULTS

Simulation I: k-space undersampling

Fig. 3 shows the within-ROI NRMSE versus XFOV diameter for each design method in Simulation I. Compared to CP, the iterative method, regardless of ROI specification, led to lower within-ROI NRMSE for all XFOV diameter values considered. When XFOV diameter was 18 cm (adequate XFOV for our desired pattern), iterative method using the circular ROI outperformed CP, whereas iterative method using the elliptic ROI outperformed CP by a slightly larger margin. The margins became significant larger when k-space was undersampled, revealing the excitation accuracy advantage by the iterative method, and the further benefit of reducing ROI size. With CP, k-space undersampling led to excitation aliasing within ROI. The iterative method was efficacious in suppressing the aliasing effect, as the effect was accounted for in the optimization cost function, and thus minimized. ROI size reduction gave extra degrees of freedom towards better excitation accuracy.

These results also suggest that a given desired excitation accuracy can be achieved with a shorter trajectory, using the iterative method instead of CP. The iteratively designed pulse at (iv) on Fig. 3 produced within-ROI accuracy close to the one by CP at (i), but its pulse length was significantly shorter (6.62 ms at (iv), 9.01 ms at (i)).

Fig. 4 shows the excitation patterns corresponding to (i)-(iv) on Fig. 3, whereas Fig. 5 displays the gradient and RF (magnitude) waveforms corresponding to (ii)-(iv). Although the same k-space trajectory was deployed, the design methods produced significantly different RF pulses. The iteratively-designed pulse at (iii) had a spike corresponding to a k-space location close to the origin, which could lead to peak power violation. Simulation III illustrates modified regularization that suppressed the spike.

Simulation II: off resonance correction

Fig. 6 shows within-ROI NRMSE in the transition region plotted against off resonance gradient magnitude. Pulses designed with CP produced increasingly distorted excitation in the transition region as the region became steeper. The degradation was consistent with results from other research studies which reported that the analogous CP reconstruction method could not correct well for rough field maps [22]. On the other hand, iteratively designed pulses were relatively immune to large off resonance gradients. The excitation performance degraded relatively slowly as the gradient increased. Specification of the elliptic ROI in the iterative method did not have much effect on excitation accuracy.

Fig. 7a shows excitation pattern by a pulse designed with CP *without* field map incorporation, at gradient magnitude 75 Hz/cm. Without field map incorporation, the pattern was blurred due to off resonance. Patterns underlying (i)-(iii) in Fig. 6 are juxtaposed in Fig. 7b-d. In regions with zero off resonance gradient, both design methods led to apparently equal excitation accuracy. Yet, off resonance gradient in the transition region differentiated the pulses. It is surprising that degradation in Fig. 7b turned out to be spatially localized.

Simulation III: RF power management

Fig. 8a shows the original pulse (blue; same pulse as in the third panel of Fig. 5), and its redesigned versions (green, red) with Tikhonov regularization parameter β incremented to 5.25 and 11.25, respectively. Tikhonov regularization influenced the entire pulse, but predominantly on its early portion corresponding to the proximity of the k-space origin. Thus, we zoom in the pulses over the first half millisecond. The potentially unrealizable spike in the original pulse was significantly reduced with $\beta = 5.25$. It shrunk by 50% with $\beta = 11.25$, as the integrated power was roughly halved relative to the original pulse. The pulses were significantly different from scaled versions of the original pulse.

Simulated profiles of these three pulses (at $y = 0$ cm) illustrated that integrated power was reduced at a low cost in excitation accuracy (Fig. 9). Scaling the original pulse by $1/\sqrt{2}$ was effective in cutting the original power by half, but the accuracy cost was significantly higher than when using Tikhonov regularization ($\beta = 11.25$).

Fig. 8b illustrates using local regularization for peak power reduction (spike suppression). The original pulse (blue) is juxtaposed with its redesigned version (red) with roughly 25% of the original peak power, computed iteratively with local regularization parameters plotted in Fig. 8c. Compared to the original pulse clipped at half maximum, the redesigned pulse was subtly different, and profile simulation (at $y = 0$ cm) revealed that it led to significantly better excitation accuracy (Fig. 10). Note also that 50% spike suppression was achieved at a lower cost via local regularization, compared to using the globally influential Tikhonov regularization.

These two examples highlight how the optimization design approach modifies each pulse sample to seek for an optimal tradeoff between pulse power and excitation accuracy.

Experiment I: variable-density trajectory

An ROI was derived from thresholding a prescanned image of the phantom (Fig. 11a-b). Fig. 11c-e are respectively the desired disc pattern, and patterns excited by two pulses designed with the CP and iterative methods. Notice the aliasing effect in the CP pattern caused by undersampling of the high spatial frequency region, which contained significant energy due to the sharp disc edges. With the iteratively designed pulse, the aliasing effect was significantly reduced, although the same trajectory was deployed. It was consistent with results of Simulation I, and likewise could be explained by inclusion of the aliasing phenomenon in the optimization cost function being minimized. Bloch simulation of the iteratively-designed pulse (Fig.11f) revealed utilization of the extra degrees of freedom in the outside-phantom region towards enhanced within-ROI accuracy.

Experiment II: off resonance correction

Fig. 12a-b show the “stripes” desired pattern and the pattern excited by an iteratively-designed pulse *before* the three metal pieces were attached to the phantom surface. Fig. 12c shows the field map of the axial plane being imaged, which was inferior to the attached pieces. It revealed global distortion of the main field. Such field inhomogeneity is comparable to, for example, that in brain regions near air cavities in the human skull. The same iteratively-designed pulse, now applied in a distorted field, excited a distorted pattern (Fig. 12d). The field map was then incorporated in the design methods. Fig. 12e-f show patterns excited by pulses designed with field-map-incorporated CP and iterative methods, respectively. The pattern distortion was significantly alleviated in both cases, but the iteratively designed pulse performed slightly better, as can be observed at regions with high off resonance gradient magnitude (white arrows). Accuracy at regions with low gradient magnitude was comparable. These observations were consistent with results in Simulation II. We expect the benefit of the iterative method to be more prominent when using longer pulses (for example, the three-dimensional tailored RF pulse in [2]).

DISCUSSION

We have formulated an optimization approach to the pulse design problem for small-tip-angle selective excitation. We have shown that it is beneficial in several ways.

In our simulations and experiments, iteratively designed pulses, which were optimal with respect to the linear design system model, produced significantly more accurate excitation patterns from the Bloch equation system, compared to the conventionally designed pulses. We found experimentally that this was generally true, despite the fact that iteratively designed pulses were not optimized with respect to the nonlinear Bloch equation. The accuracy benefit was particularly prominent when the trajectory undersampled k-space (either partially or entirely), since aliasing was taken into account by the optimization scheme when it sought the cost-minimizing pulse. This im-

portant feature makes the iterative method stand out from non-iterative ones. Secondly, iteratively designed pulses excited more accurately at spatial regions with large off resonance gradients. This was partially attributable to the obviation of DCF evaluation in the design process. As mentioned at the beginning, accurate DCF determination is generally difficult in the presence of large off resonance gradients, and DCF errors contribute significantly to excitation error. The iterative method simply does not require the separate task of DCF evaluation.

We have also shown the use of excitation error weighting for controlling excitation precision at different spatial regions. With the iterative method, designers can assign zero weights to “don’t-care” regions and large weights to ROIs. In particular, assigning “don’t-care” labels to uninteresting body regions, or regions where there is zero or low spin density (for example, outside-body regions), can boost precision in the ROI.

In addition to precision improvement, the iterative method can potentially lead to shorter pulse lengths, as undersampled k-space can be used at lower penalty of excitation accuracy. In some applications (for example, [2]), slightly compromised overall excitation precision may be more tolerable than exceedingly lengthy pulses. Lastly, regularization can be used to trade excitation accuracy for reduction in integrated and peak RF power. The global Tikhonov and local regularization techniques enable the designer to avoid suboptimal strategies to make pulses implementable (for example, scaling or clipping). RF power management can be crucial in pulse design problems in high-field MRI.

The cost of all the benefits above is an increase in algorithm complexity, and thus computational time. However, computational time was only a minor issue for our two-dimensional designs. On our Linux system with a 3.2GHz processor and 2GB memory, the 15-iteration computation of the pulses in Fig. 5 took only 7.07 seconds. However, computational time (and memory) required for pulse designs for volumetric selective excitation (for example, [2, 7]) could be an issue. Algorithm acceleration can be achieved via time and frequency segmentation schemes [9, 22, 33], which make approximations to the off-resonance exponential factor in Eq. (3) so that the fast Fourier transformation (FFT) can be utilized. These acceleration techniques are currently under investigation.

Interesting extensions of the optimization approach include the possible *joint* optimization of the excitation k-space trajectory and RF pulse for a given desired pattern, as inspired by the work of Hardy *et al.* [20]. Future success towards this direction could potentially lead to significant reduction in RF pulse length. Another extension direction would be to incorporate physical phenomena, such as spatial variations in RF coil sensitivity and RF field homogeneity, in the optimization formulation. Small-tip-angle selective excitation in multi-coil transmit systems [5, 6] and high-field imaging would benefit readily.

At a low cost in computational time, the iterative RF pulse design method is advantageous in terms of excitation precision, DCF obviation, potential pulse length reduction and pulse power management. Our approach can benefit current applications of small-tip-angle selective excitation, and possibly foster future ones.

APPENDIX

Solution to the inequality-constrained optimization problem

The inequality-constrained optimization problem described by Eqs. (8) and (9) can be solved using the *Karush-Kuhn-Tucker* (KKT) Theorem. The theorem states that if \mathbf{b}^* is a *regular point* and a local minimizer to the problem, there exists non-negative real *Lagrange multipliers* $\{\lambda_j^*\}_{j=0}^{N_t-1}$ such that for $j = 0, \dots, N_t - 1$,

$$\lambda_j^* \cdot (|b_j^*|^2 - C) = 0, \quad (11)$$

and the gradient of the *Lagrangian function* evaluated at \mathbf{b}^* equals $\mathbf{0}$:

$$\nabla \{ \|\mathbf{A}\mathbf{b}^* - \mathbf{d}\|_{\mathbf{W}}^2 + \beta \mathbf{b}^{*\prime} \mathbf{b}^* + \sum_{j=0}^{N_t-1} \lambda_j^* (|b_j^*|^2 - C) \} = \mathbf{0}. \quad (12)$$

Eqs. (11) and (12) have to be solved simultaneously for the optimizer. One can use commercial optimization packages (for example, Optimization Toolbox in Matlab) to tackle the problem, although conversion of the problem to a real-valued one may be necessary, and the process can be computationally expensive. If the multipliers are known *a priori*, \mathbf{b}^* can be obtained, due to the convexity of the Lagrangian function, via

$$\mathbf{b}^* = \arg \min_{\mathbf{b}} \{ \|\mathbf{A}\mathbf{b} - \mathbf{d}\|_{\mathbf{W}}^2 + \beta \mathbf{b}' \mathbf{b} + \mathbf{b}' \mathbf{\Lambda}^* \mathbf{b} \}, \quad (13)$$

where $\mathbf{\Lambda}^* = \text{diag}(\lambda_j^*)$.

ACKNOWLEDGEMENT

The authors would like to thank the National Institute of Health (NIH) for funding (Grant: R01 DA15410), and Professor Matthew O'Donnell and Professor Romesh Saigal of University of Michigan for helpful discussions.

References

- [1] Pauly JM, Nishimura DG, and Macovski A. A k-space analysis of small-tip-angle excitation. *J Magn Reson*, 81:43–56, 1989.
- [2] Stenger VA, Boada FE, and Noll DC. Three-dimensional tailored RF pulses for the reduction of susceptibility artifacts in T_2^* -weighted functional MRI. *Magn Reson Med*, 44:525–531, 2000.
- [3] Rieseberg S, Frahm J, and Finsterbusch J. Two-dimensional spatially-selective RF excitation pulses in echo-planar imaging. *Magn Reson Med*, 47:1186–1193, 2002.
- [4] Mohiaddin RH, Gatehouse D, Moon JC, Youssuffidin M, Yang GZ, Firmin DN, and Pennell DJ. Assessment of reactive hyperaemia using real time zonal echo-planar flow imaging. *J Cardiovasc Magn Reson*, 4:283–287, 2002.

- [5] Katscher U, Börnert P, Leussler C, and van den Brink JS. Transmit SENSE. *Magn Reson Med*, 49:144–150, 2003.
- [6] Zhu Y. Parallel excitation with an array of transmit coils. *Magn Reson Med*, 51:775–784, 2004.
- [7] Saekho S, Boada FE, Noll DC, and Stenger VA. Small tip angle three-dimensional tailored radiofrequency slab-select pulse for reduced B1 inhomogeneity at 3 T. *Magn Reson Med*, 53(2):479–484, 2005.
- [8] Pauly JM, Nishimura DG, and Macovski A. A linear class of large-tip-angle selective excitation pulses. *J Magn Reson*, 82:571–587, 1989.
- [9] Noll DC, Meyer CH, Pauly JM, Nishimura DG, and Macovski A. A homogeneity correction method for magnetic resonance imaging with time-varying gradients. *IEEE Trans Med Imag*, 10(4):629–637, 1991.
- [10] Schomberg H. Off-resonance correction of MR images. *IEEE Trans Med Imag*, 18(6):481–495, 1999.
- [11] Börnert P and Aldefeld B. On spatially selective RF excitation and its analogy with spiral MR image acquisition. *Magn Reson Materials in Phys, Bio and Med*, 7:166–178, 1998.
- [12] Schomberg H and Börnert P. Off-resonance correction of nD spatially selective RF pulses. In *Proceedings of the 6th Annual Meeting of ISMRM, Sydney, 1998*, page 2059.
- [13] Noll DC, Fessler JA, and Sutton BP. Conjugate phase MRI reconstruction with spatially variant sample density correction. *IEEE Trans Med Imag*, 24(3):325–336, 2005.
- [14] Pipe JG and Menon P. Sampling density compensation in MRI: rationale and an iterative numerical solution. *Magn Reson Med*, 41:179–186, 1999.
- [15] Conolly S, Nishimura DG, and Macovski A. Optimal control solutions to the magnetic resonance selective excitation problem. *IEEE Trans Med Imag*, MI-5(2):106–115, 1986.
- [16] Murdoch JB, Lent AH, and Kritzer MR. Computer-optimized narrowband pulses for multislice imaging. *J Magn Reson*, 74:226–263, 1987.
- [17] Conolly S. *Magnetic resonance selective excitation*. PhD thesis, Stanford University, CA, 1989.
- [18] Lurie DJ. A systematic design procedure for selective pulses in NMR imaging. *Magn Reson Imag*, 3:235–243, 1985.
- [19] O’Donnell M and Adams WJ. Selective time-reversal pulses for NMR imaging. *Magn Reson Imag*, 3:377–382, 1985.
- [20] Hardy CJ, Bottomley PA, O’Donnell M, and Roemer P. Optimization of two-dimensional spatially selective NMR pulses by simulated annealing. *J Magn Reson*, 77:233–250, 1988.
- [21] Harshbarger TB and Twieg DB. Iterative reconstruction of single-shot spiral MRI with off resonance. *IEEE Trans Med Imag*, 18(3):196–205, 1999.
- [22] Sutton BP, Noll DC, and Fessler JA. Fast, iterative image reconstruction for MRI in the presence of field inhomogeneities. *IEEE Trans Med Imag*, 22(2):178–188, 2003.
- [23] Munger P, Crelier GR, Peters TM, and Pike GB. An inverse problem approach to the correction of distortion in EPI images. *IEEE Trans Med Imag*, 19(7):681–689, 2000.

- [24] Bazaraa MS, Sherali HD, and Shetty CM. *Nonlinear Programming*. Wiley, New York, 2nd edition, 1993.
- [25] Glover GH. Simple analytic spiral K-space algorithm. *Magn Reson Med*, 42:412–415, 1999.
- [26] Spielman D, Pauly J, Macovski A, and Enzmann D. Spectroscopic imaging with multidimensional pulses for excitation:SIMPLE. *Magn Reson Med*, 19:67–84, 1991.
- [27] Hoge RD, Kwan RK, and Pike GB. Density compensation functions for spiral MRI. *Magn Reson Med*, 38:117–128, 1997.
- [28] Schneider E and Glover GH. Rapid in vivo proton shimming. *Magn Reson Med*, 18:335–347, 1991.
- [29] Schröder C, Börnert P, and Aldefeld B. Spatial excitation using variable-density spiral trajectories. *J Magn Reson Imag*, 18:136–141, 2003.
- [30] Stenger VA, Boada FE, and Noll DC. Variable-density spiral 3D tailored RF pulses. *Magn Reson Med*, 50:1100–1106, 2003.
- [31] Nehrke K, Börnert P, Groen J, Smink J, and Böck JC. On the performance and accuracy of 2D navigator pulses. *J Magn Reson Imag*, 17(8):1173–1181, 1999.
- [32] Fessler JA. Penalized weighted least-squares image reconstruction for positron emission tomography. *IEEE Trans Med Imag*, 13(2):290–300, 1994.
- [33] Man LC, Pauly JM, and Macovski A. Multifrequency interpolation for fast off-resonance correction. *Magn Reson Med*, 37:785–792, 1997.

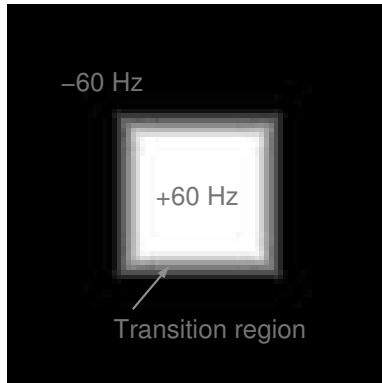


Figure 1. Field map incorporated in the Bloch simulator and design methods in Simulation II.

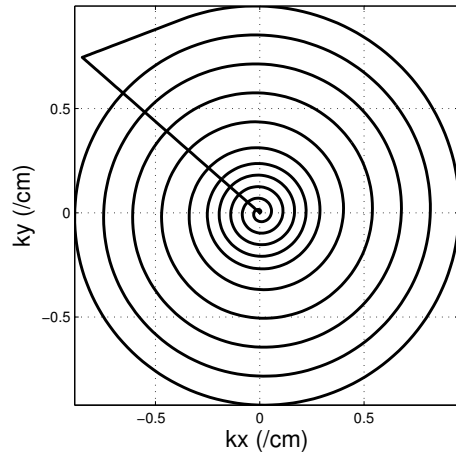


Figure 2. Variable-density spiral trajectory deployed in Scanner Experiment I.

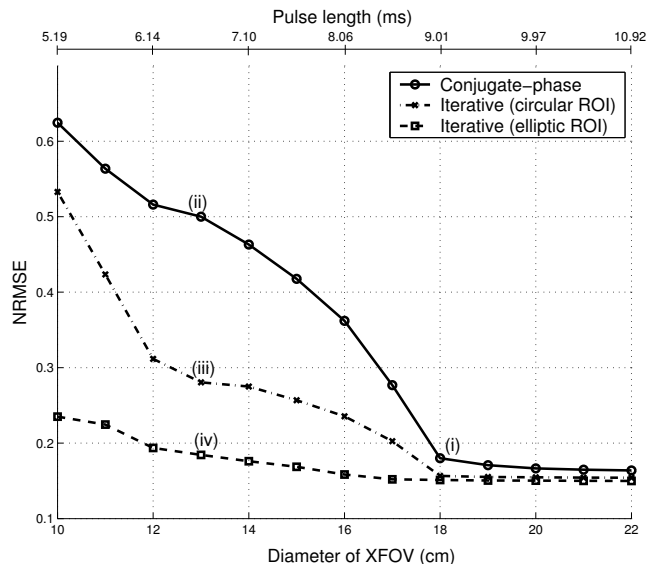


Figure 3. Within-ROI excitation error resulting from RF pulses designed for spiral trajectories with different XFOV (resolution held fixed). For a given trajectory, higher excitation accuracy was achieved by the iterative method, especially when the trajectory undersampled k-space. Reduction in size of ROI in the iterative method led to better within-ROI accuracy and higher tolerance of k-space undersampling. The excitation patterns and pulses at points (i)-(iv) are shown in Fig. 4 and 5.

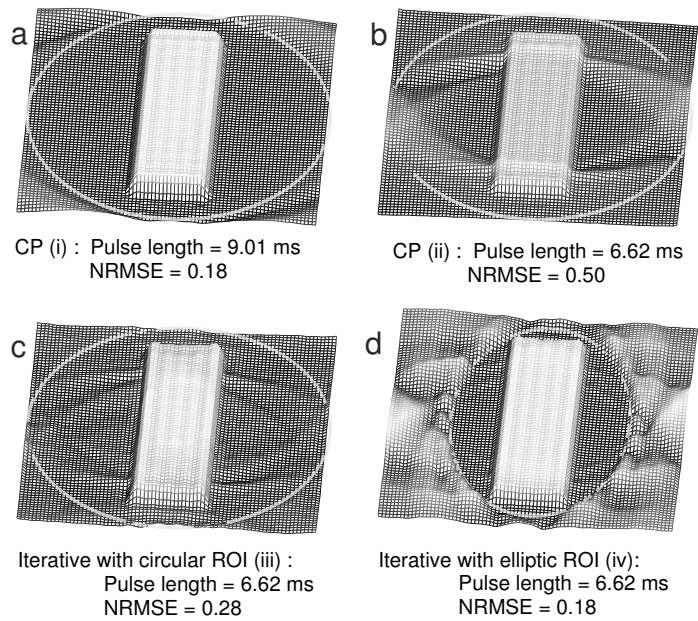


Figure 4. Simulated excitation patterns corresponding to points (i)-(iv) in Fig. 3, respectively. Interior regions of the solid lines represent the circular or elliptic ROI. a: Pattern by an adequately-sampling trajectory and a CP-designed pulse (i). b-d: Patterns by a common trajectory that undersampled k-space ($XFOV = 13$ cm), accompanied by pulses designed with CP (ii) or the iterative method, with different ROI specification (iii,iv).

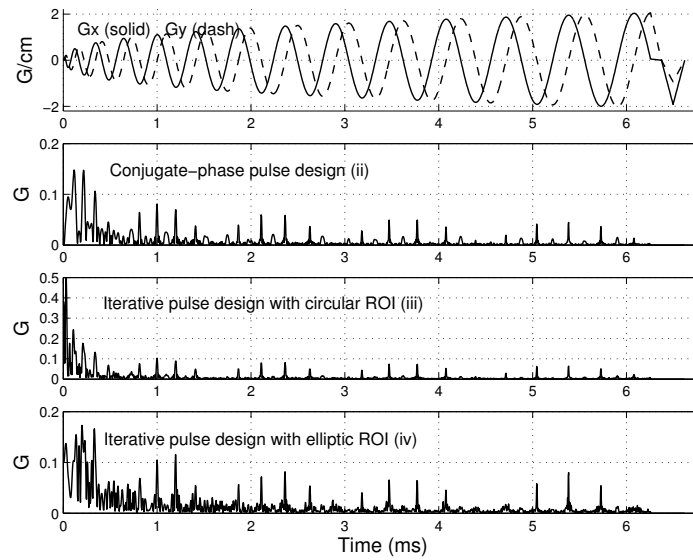


Figure 5. Gradient and RF (magnitude) waveforms used to produce excitation patterns in Fig. 4b-d, corresponding to points (ii)-(iv) in Fig. 3. Despite the same gradient waveforms and desired pattern in use, the RF pulse designs differed significantly. (G: Gauss)

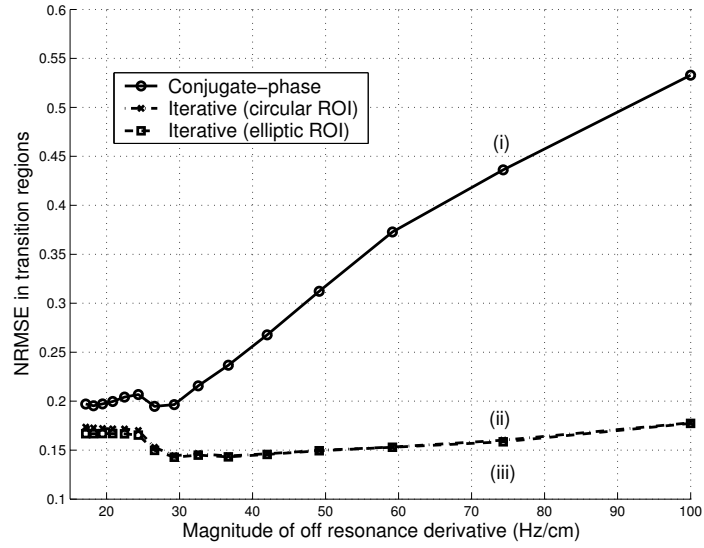


Figure 6. NRMSE in the transition region within ROI, versus the region's steepness. As the transition became more rapid, performance of the CP-designed pulses degraded, whereas the iteratively designed pulses were relatively immune. Fig. 7 shows excitation patterns at points (i)-(iii).

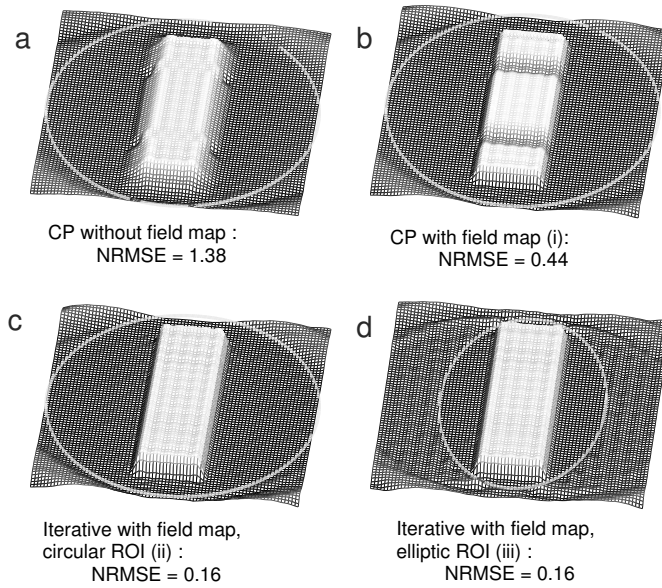


Figure 7. a: Simulated excitation pattern by a pulse designed using CP without incorporation of the field map in the simulator, with transition region at 75 Hz/cm. b-d: Patterns by pulses designed with field-map-incorporated CP (point (i) in Fig. 6) or iterative method, with different ROI specification (ii,iii). Interior regions of the solid lines represent the circular or elliptic ROI.

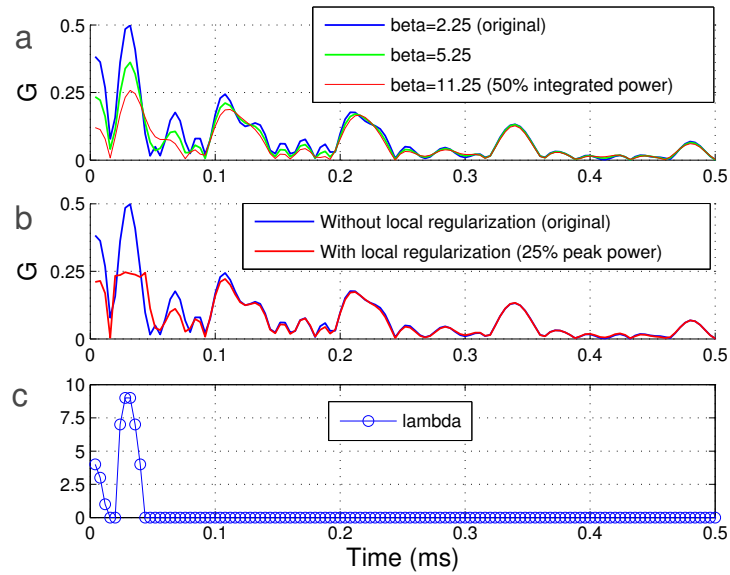


Figure 8. a: The original pulse (blue; same pulse as in third panel in Fig. 5) designed with Tikhonov regularization ($\beta = 2.25$). The pulse over the first half millisecond is plotted. Incrementing β reduced the spike height and integrated pulse power (green, red). b: Original pulse (blue), and the pulse redesigned with local regularization. Its peak power was about 25% of the original. c: The local regularization parameters used for the redesigned pulse in b. (Note: pulse magnitude is plotted in Gauss (G).)

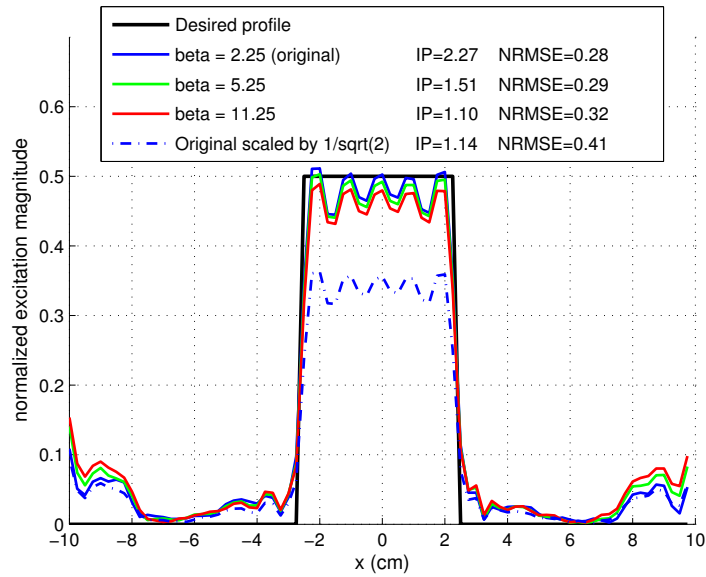


Figure 9. Simulated pattern profiles at $y = 0$ cm, created by the original pulse (blue in Fig. 8a), the pulses redesigned with increased Tikhonov regularization (green, red in Fig. 8a) and the original pulse scaled by $1/\sqrt{2}$. With regularized iterative design method, integrated power (IP) reduction was achieved with low penalty in excitation accuracy. (Note: IP is in arbitrary units.)

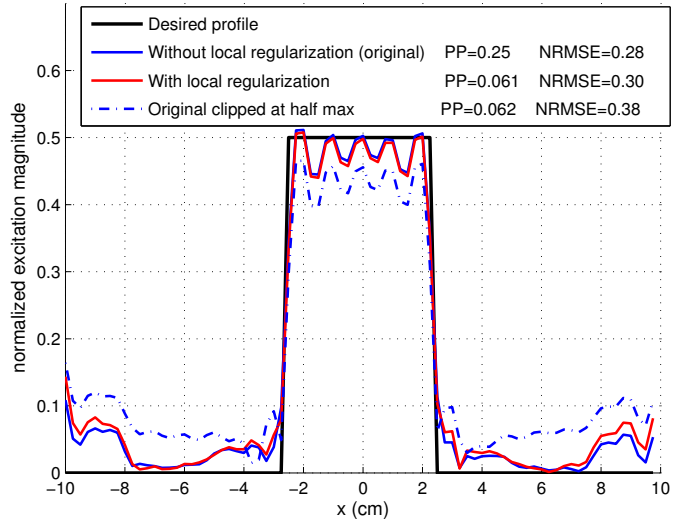


Figure 10. Simulated pattern profiles at $y = 0$ cm, created by the original pulse (blue in Fig. 8b), the pulse (red in Fig. 8b) redesigned with local regularization parameters in Fig. 8c, and the original pulse clipped at half maximum. With regularized iterative design method, peak power (PP) reduction was achieved with a low penalty in excitation accuracy. (Note: PP is in arbitrary units.)

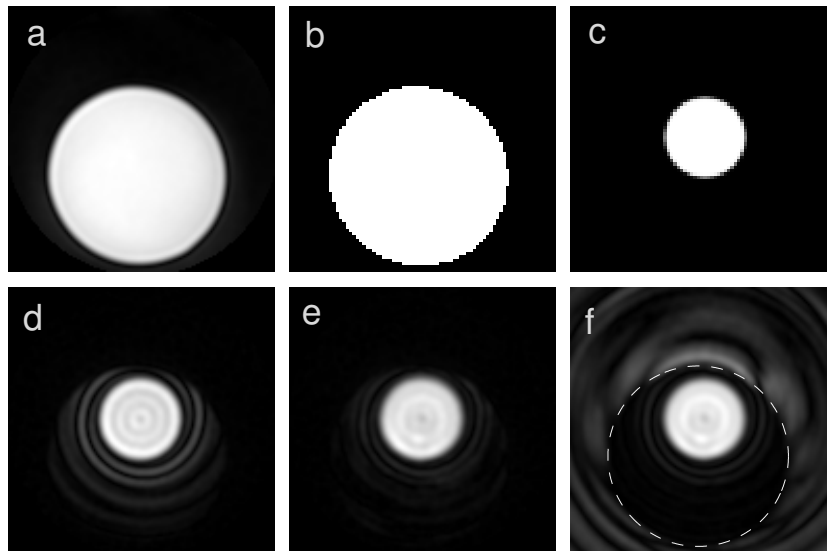


Figure 11. a,b: Prescanned image and ROI obtained by thresholding, respectively. c: Desired pattern. d: Measured pattern excited by CP-designed pulse, plagued by aliasing excitation. e: Measured pattern excited by pulse designed with ROI-incorporated iterative method. Compared to the CP case, aliasing was significantly alleviated. f: Bloch simulation result of the iteratively-designed pulse used in e (dash line: ROI).

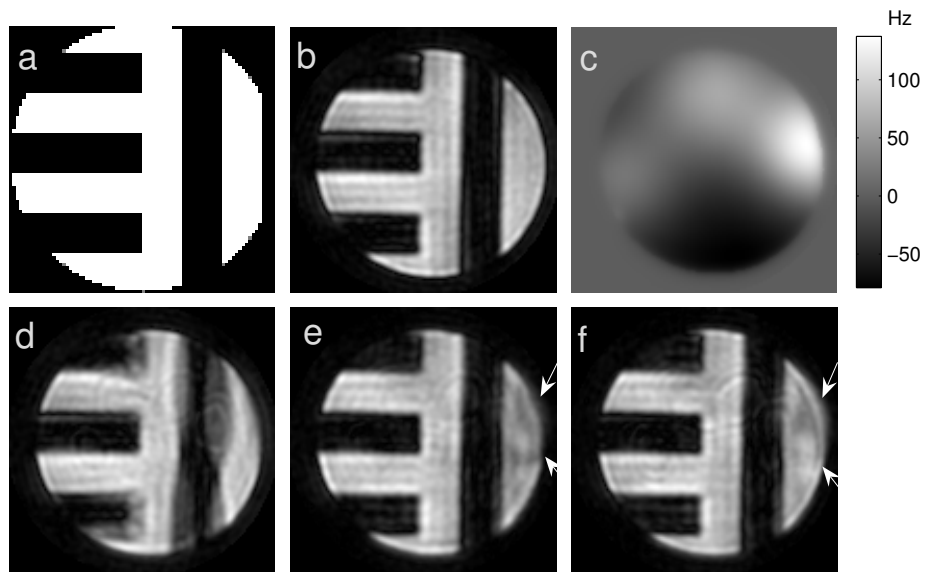


Figure 12. a: Desired excitation pattern. b: Pattern by iteratively-designed pulse, before metal pieces were attached to the phantom. c: Field map after attachment of the metal pieces. d: Pattern by pulse in b, distorted due to the inhomogenous field. e: Pattern by pulse designed with CP with field map incorporation. f: Pattern by pulse iteratively designed, with field map incorporation. Field correction by the iterative method was slightly better at regions with high off resonance gradient (white arrows).

Footnotes

1. The RF pulse being physically played out can be modeled as a pulse sample weighted “train of Dirac impulses”, convolved with a time-invariant point spread function. The temporal spreading can arise from D/A converter characteristics and RF circuit impulse response functions. We ignore this spreading effect in the analysis here though it could be incorporated easily.

List of symbols

- \mathbf{M} : transverse plane magnetization pattern (complex, continuous function of space)
- \mathbf{x} : spatial location
- \mathbf{b} : RF pulse envelope (complex, continuous function of time)
- \mathbf{g} : gradient waveforms (real, continuous vector function of time)
- t : time
- T : end time of the excitation waveforms
- M_o : equilibrium magnetization magnitude
- \mathbf{D} : desired transverse plane magnetization pattern (complex, continuous function of space)
- \mathbf{W} : error weighting pattern (real, continuous function of space)
- β : Tikhonov regularization parameter
- \mathbf{C} : pulse magnitude constraint bound, dependent on RF amplifier peak power limitation
- γ : gyromagnetic ratio
- \mathbf{k} : excitation k-space trajectory
- $\Delta\omega$: resonance frequency offset
- $\{b_j\}$: RF pulse samples in pulse sequence
- Δt : sampling period of the RF pulse samples
- N_t : number of time samples
- N_s : number of space samples
- \mathbf{A} : system matrix
- $\{a_{ij}\}$: elements of system matrix
- \mathbf{b} : RF pulse (complex vector)
- \mathbf{m} : transverse plane magnetization pattern (complex vector)
- $\hat{\mathbf{b}}$: RF pulse designed by the iterative method (complex vector)
- \mathbf{W} : diagonal error weighting matrix
- $\{\lambda_j\}$: Lagrange multipliers (pointwise regularization parameters)
- Λ : diagonal matrix $diag(\lambda_j)$
- $\mathbf{R} : \mathbf{I}\beta + \Lambda$

- $\hat{\mathbf{b}}^{(n)}$: pulse design from the n -th iterate of the CG algorithm
- $\tilde{\mathbf{m}}$: variable within the CG algorithm
- O : computational complexity order